

Supplementary Materials

Novel strongly luminescent diketofurofuran (DFF) dye in liquid crystal matrices for thermal sensors and light amplification

M. Czajkowski^{a,*}, Ł. Duda^{a,b,†}, S. J. Czarnocki^{a,†}, A. B. Szukalska^c, M. Guzik^{a,b}, J. Myśliwiec^c,
M. Skoreński^a, B. Potaniec^a, J. Cybińska^{a,b,*}

^aŁukasiewicz Research Network – PORT Polish Center for Technology Development, ul. Stabłowicka 147,
54-066 Wrocław, Poland

* e-mails: maciej.czajkowski@port.lukasiewicz.gov.pl, joanna.cybinska@port.lukasiewicz.gov.pl

^bUniversity of Wrocław, Faculty of Chemistry, ul. Joliot-Curie 14, 50-383 Wrocław, Poland

^cWrocław University of Science and Technology, Faculty of Chemistry, Wybrzeże Wyspiańskiego 29,
50-370 Wrocław, Poland

† the authors contributed equally to this work

S1. Synthesis of dyes and LC host

S1.1 General experimental information on synthesis

All reactions were carried out in flasks under inert argon atmosphere and were stirred magnetically. Anhydrous solvents were used under inert argon atmosphere. All other chemicals were used as supplied. Column chromatography was carried out using *Macherey-Nagel Kieselgel 60* (40–63 μm). Analytical thin layer chromatography was carried out using *DC Kieselgel 60 F₂₅₄* aluminium sheets coated with silica gel. Components were visualized using ultraviolet light. The nuclear magnetic resonance spectra (¹H and ¹³C) were recorded on *NMR Avance III HD 500 MHz or NMR Avance III HD 600 MHz* (Bruker, Billerica, MA, USA) spectrometers. Chemical shifts are given in ppm, relative to internal standard—tetramethylsilane (TMS); all *J* values are in Hz. The high-resolution Electrospray Ionization Mass Spectroscopy (ESI-HRMS) spectra were measured on a *ESI-Q-TOF Maxis Impact Mass Spectrometer* (Bruker, Billerica, MA, USA).

S1.2. Synthesis of 3,6-bis(4-(hexyloxy)phenyl)furo[3,4-c]furan-1,4-dione (6O,6O-DFF)

The path for synthesis of the 6O,6O-DFF dye is shown in Fig. 2 in the main text.

S1.2.1. 4-(Hexyloxy)benzonitrile (2)

The solution of 4-cyanophenol (**1**) (20 g, 168 mmol) in acetonitrile was treated with potassium carbonate (2 eq., 338 mmol, 47 g) and 1-bromohexane (1.2 eq., 202 mmol, 28.4 mL) and stirred at 80 °C for 20 hours. The solid was filtered off and the solution was partitioned between ethyl acetate and 1 N HCl. The organic phase was washed with brine, dried over Na₂SO₄, filtered and the solvent was removed to give compound (**2**) (34.2 g >100%).

¹H NMR (500 MHz, CDCl₃) δ [ppm]: 7.59 – 7.53 (m, 2H), 6.96 – 6.89 (m, 2H), 3.99 (t, *J* = 6.6 Hz, 2H), 1.85 – 1.74 (m, 2H), 1.51 – 1.41 (m, 2H), 1.39 – 1.27 (m, 4H), 0.96 – 0.86 (m, 3H).

¹³C NMR (126 MHz, CDCl₃) δ 162.5, 134.0, 119.3, 115.2, 103.7, 68.4, 31.5, 29.0, 25.6, 22.6, 14.0.

¹H NMR and ¹³C NMR spectra of (**2**) are presented in Fig. S1.

ESI-HRMS (+): Calculated for: C₁₃H₁₇NONa 226.1202. Found *m/z* 226.1214 [M+Na]⁺. The spectroscopic data are supported by the literature [1].

S1.2.2. Ethyl 3-(4-(hexyloxy)phenyl)-3-oxopropanoate (3).

The procedure for the synthesis of (**3**) was adapted from the literature [2]. To a stirred suspension of zinc dust (2 eq, 19.2 g, 295 mmol) in THF (60 mL) was added MeSO₃H (50 mg, 0.5 mmol) at RT. The mixture was refluxed for 10 min and 4-hexyloxybenzonitrile (**2**) (1 eq, 30 g, 63 mmol) was added. To the mixture was added ethyl bromoacetate (1.6 eq, 39.4 g, 236 mmol) over 1 h. After 30 min, the mixture was cooled to 0 °C and aq 3 N HCl (40 mL) was added dropwise. After 2 h, all the organic volatiles were removed in vacuo and the remaining mixture was extracted with EtOAc (60 mL). The separated organic

¹ N. Cox, H. Dang, A. M. Whittaker and G. Lalic, *Tetrahedron*, 2014, **70**, 4219.

² H. Shin, B. S. Choi, K. K. Lee, H.-W. Choi, J. H. Chang, K. W. Lee, D. H. Nam and N.-S. Kim, *Synthesis*, 2004, **16**, 2629.

layer was washed with H₂O, dried (Na₂SO₄) and concentrated. Column chromatography (EtOAc–cyclohexane, 1:20, v/v) of the residue afforded 24 g (55%) of **(3)** as a colourless oil.

¹H NMR (500 MHz, CDCl₃) δ [ppm]: 7.95 – 7.86 (m, 2H), 6.95 – 6.89 (m, 2H), 4.20 (q, J = 7.1 Hz, 2H), 4.02 (t, J = 6.6 Hz, 2H), 3.93 (s, 2H), 1.85 – 1.74 (m, 2H), 1.52 – 1.41 (m, 2H), 1.40 – 1.29 (m, 4H), 1.25 (t, J = 7.1 Hz, 2H), 0.94 – 0.88 (m, 3H).

¹³C NMR (126 MHz, CDCl₃) δ 191.0, 167.8, 163.7, 130.9, 128.9, 114.4, 68.4, 61.4, 45.8, 31.5, 29.0, 25.6, 22.6, 14.1, 14.0.

¹H NMR and ¹³C NMR spectra of **(3)** are presented in Fig. S2.

ESI-HRMS (+): Calculated for: C₁₇H₂₄O₄Na 315.1567. Found *m/z* 315.1578 [M+Na]⁺.

S1.2.3. Diethyl 2,3-bis(4-(hexyloxy)benzoyl)succinate (**4**).

A solution of **(3)** (14 g, 48 mmol) in 40 mL of dry ether was added to a suspension of sodium metal (1.1 g, 48 mmol) in ether (100 mL), and the mixture was stirred overnight under nitrogen. A solution of iodine (6.08 g, 24 mmol) in ether (30 mL) was added in small portions with vigorous stirring. The mixture was stirred for 2 h, and a saturated solution of sodium thiosulfate (30 mL) was added. The organic phase was separated, dried (Na₂SO₄), and evaporated. 11 g (79%) of **(4)** was obtained as a colourless oil. The product was used for the next step without further purification.

S1.2.4. 3,6-bis(4-(hexyloxy)phenyl)furo[3,4-c]furan-1,4-dione (**5**) (*6O,6O-DFP*).

Procedures for synthesis of **(5)** were adapted from the literature^[3,4]. Diethyl-2,3-bis(4(hexyloxy)-benzoyl)succinate (**4**) (2.78 g, 7.51 mmol) was slowly heated in vacuo (290–300 °C). After cooling down, the brown material was refluxed with methanol (30 mL) and filtered. The residue was recrystallized from dichloromethane to furnish 1.02 g (47%) of orange crystals.

¹H NMR (500 MHz, CDCl₃) δ [ppm]: 8.21 (d, J = 8.9 Hz, 4H), 7.03 (t, J = 7.5 Hz, 4H), 4.07 (t, J = 6.6 Hz, 4H), 1.82 (dt, J = 14.4, 6.6 Hz, 4H), 1.52 – 1.42 (m, 4H), 1.40 – 1.32 (m, 8H), 0.95 – 0.88 (m, 6H).

¹³C NMR (126 MHz, CDCl₃) δ 163.5, 159.2, 155.7, 130.5, 119.0, 115.4, 106.8, 68.6, 31.5, 29.0, 25.6, 22.6, 14.0.

¹H NMR and ¹³C NMR spectra of **(5)** are presented in Fig. S3.

ESI-HRMS (+): Calculated for C₃₀H₃₄O₆Na: 513.2248. Found *m/z* 513.2255 [M+Na]⁺.

The mid-infrared absorption spectrum of the *6O,6O-DFP* dye measured by ATR FT-IR technique can be found in Fig. S4. Determined stability temperature of the *6O,6O-DFP* dye by thermogravimetric analyser TGA2 (Mettler Toledo) at heating cycle 10°C/min is 360°C (onset value).

S1.3. Synthesis of 3,6-bis(4-octyloxyphenyl)-2,5-dimethyl-2,5-dihydropyrrolo[3,4-c]pyrrole-1,4-dione (*8O,8O-dMeDPP*).

In a first step, a precursor compound – *8O,8O-DPP* was synthesized, which is not substituted (with methyl groups) at nitrogen atoms with respect to the *8O,8O-dMeDPP* dye.

S1.3.1. Synthesis of 3,6-bis(4-octyloxyphenyl)-2,5-dihydropyrrolo[3,4-c]pyrrole-1,4-dione (*8O,8O-DPP*)

The three-neck round bottom flask was filled with nitrogen, then potassium *tert*-butoxide (2.53 g, 22.5 mmol) was placed. Under the stream of nitrogen 4-(octyloxy)benzocyanide (4.00 g, 18.0 mmol) dissolved in 35 mL of *tert*-amyl alcohol (TAA) was added. The mixture was gently heated to boiling and the diisopropyl succinate (1.46 g, 7.20 mmol) dissolved in 15 mL of TAA has been added for 1 hour. The change of colour to red was observed. The reaction was heated for 8 hours on a magnetic stirrer under a nitrogen atmosphere. Next, 30 mL of methanol and 30 mL of glacial acetic acid were added and the mixture was refluxed for 10 min. After cooling, the reaction mixture was poured into cold water to obtain a red precipitate (2.00 g, 3.67 mmol, 20.7% yield), which was used in the next reaction without further purification.

³ A. L. Kanibolotsky, F. Vilela, J. C. Forgie, S. E. T. Elmasly, P. J. Skabara, K. Zhang, B. Tieke, J. McGurk, C. R. Belton, P. N. Stavrinou and D. D. C. Bradley, *Adv. Mater.*, 2011, **23**, 2093.

⁴ K. Zhang and B. Tieke, *Macromol.*, 2008, **41**(20), 7287.

S.1.3.2. Synthesis of 3,6-bis(4-octyloxyphenyl)-2,5-dimethyl-2,5-dihydropyrrolo[3,4-c]pyrrole-1,4-dione (*8O,8O-dMeDPP*)

A mixture of *8O,8O-DPP* from the previous reaction (0.50 g, 0.92 mmol), methyl iodide (0.71 g, 5.0 mmol), cesium carbonate (1.6 g, 5.0 mmol), 4-(dimethylamino)pyridine (11 mg, 0.092 mmol) and 18-crown-6 (24 mg, 0.092 mmol) and *N,N*-dimethylformamide (25 mL) were placed in teflon microwave vessel. The reaction mixture was heated in a microwave reactor for 1 hour at 100 °C. In the next step, the mixture was cooled and poured into 100 mL of cold water to obtain a red precipitate. The crude product was filtered and purified using column chromatography using mixture of n-hexane:ethyl acetate 3:1 (v/v) as eluent to obtain a pure product in a form of red crystals (200 mg, 0.349 mmol, 38.0% yield).

¹H NMR (600 MHz, CDCl₃) δ (ppm): 7.93 – 7.86 (m, 4H), 7.05 – 6.98 (m, 4H), 4.04 (t, *J* = 6.6 Hz, 4H), 3.36 (s, 6H), 1.84 – 1.79 (m, 4H), 1.50 – 1.45 (m, 4H), 1.37 – 1.27 (m, 16H), 0.90 (t, *J* = 6.9 Hz, 6H);

¹³C NMR (151 MHz, CDCl₃) δ (ppm): 163.0, 161.6, 147.9, 131.2, 120.5, 114.9, 108.3, 68.4, 32.0, 29.7, 29.5, 29.4, 29.3, 26.2, 22.8, 14.2.

¹H NMR and ¹³C NMR spectra of *8O,8O-dMeDPP* are presented in Fig. S5.

ESI-HRMS (+): Calculated for C₃₆H₄₈O₂N₄: 573.3687 Found *m/z* 573.3679 [M+H]⁺.

Structure of the *8O,8O-dMeDPP* dye is presented in Fig. 1 in the main text. The spectroscopic data are supported by the literature. Determined stability temperature of the *8O,8O-dMeDPP* dye by thermogravimetric analyser TGA2 (Mettler Toledo) at heating cycle 10 °C/min is 408°C (onset value).

S1.4. Synthesis of 4'-(hexadecyloxy)-[1,1'-biphenyl]-4-carbonitrile (*16OCB*).

The structure of the LC host synthesized in this work – 4'-(hexadecyloxy)-[1,1'-biphenyl]-4-carbonitrile (*16OCB*) is given in Fig. 1a. For the synthesis a solution of 4'-Hydroxybiphenyl-4-carbonitrile (1.05 g, 5.4 mmol) in acetonitrile was treated with potassium carbonate (2 eq., 10.8 mmol, 1.5 g) and 1-bromohexadecane (1.2 eq., 6 mmol, 1.83 g) and stirred at 80°C for 20 hours. The solid was filtered off and the solution was partitioned between ethyl acetate and 1 N HCl. The organic phase was washed with brine, dried over Na₂SO₄, filtered and the solvent was removed. The crude product was recrystallized from methanol to give 2.04 g, (90%) 4'-hexadecanoxybiphenyl-4-carbonitrile as a white solid.

¹H NMR (500 MHz, CDCl₃) δ [ppm]: 7.74 – 7.69 (m, 2H), 7.68 – 7.62 (m, 2H), 7.59 – 7.51 (m, 2H), 7.06 – 6.98 (m, 2H), 4.03 (t, *J* = 6.6 Hz, 2H), 1.89 – 1.77 (m, 2H), 1.56 – 1.45 (m, 2H), 1.43 – 1.26 (m, 24H), 0.91 (t, *J* = 7.0 Hz, 3H).

¹³C NMR (126 MHz, CDCl₃) δ 159.9, 145.3, 132.6, 131.2, 128.3, 127.1, 119.1, 115.1, 110.1, 68.2, 32.0, 29.7 (3 carbons), 29.6 (2 carbons), 29.4 (2 carbons), 29.2, 26.0, 22.7, 14.1.

¹H NMR and ¹³C NMR spectra of *16OCB* are presented in Fig. S6.

ESI-HRMS (+): Calculated for C₂₉H₄₁NONa: 442.3080. Found *m/z* 442.3086 [M+Na]⁺.

Structure of the *16OCB* liquid crystal is presented in Fig. 1 in the main text.

S1.5. Spectra of the synthesized compounds

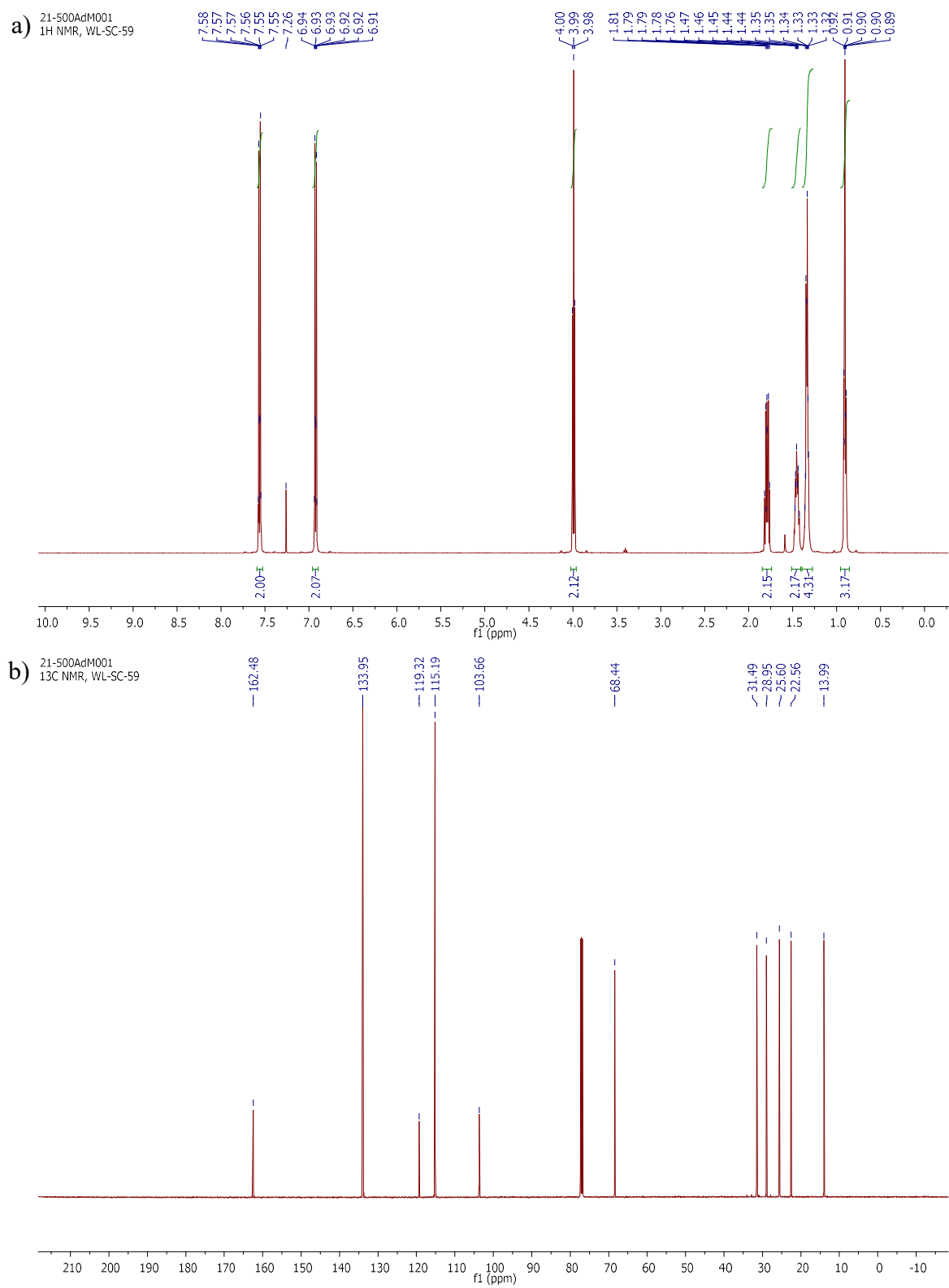


Figure S1 ¹H (a) and ¹³C NMR (b) spectra of synthesized 4-(Hexyloxy)benzonitrile (**2**).

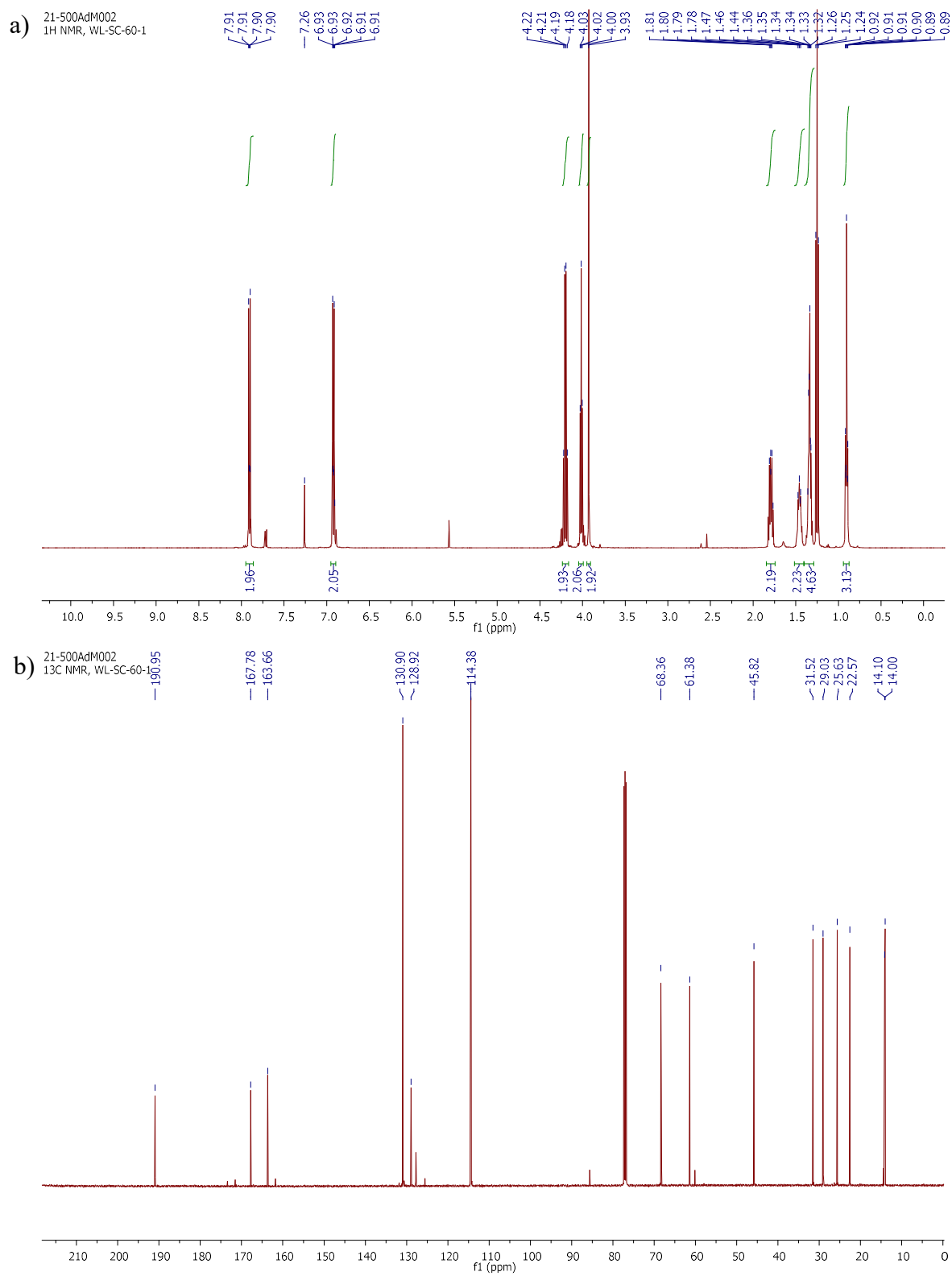


Figure S2 ¹H (a) and ¹³C NMR (b) spectra of synthesized Ethyl 3-(4-(hexyloxy)phenyl)-3-oxopropanoate (**3**).

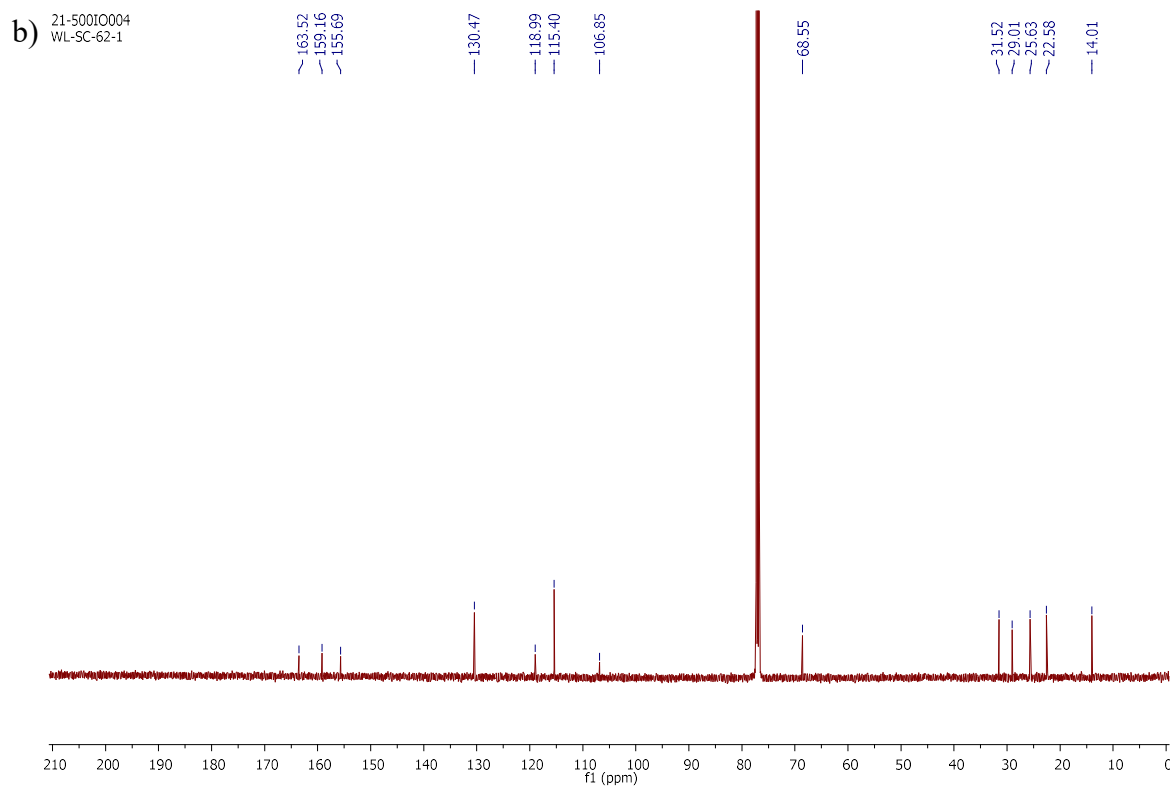
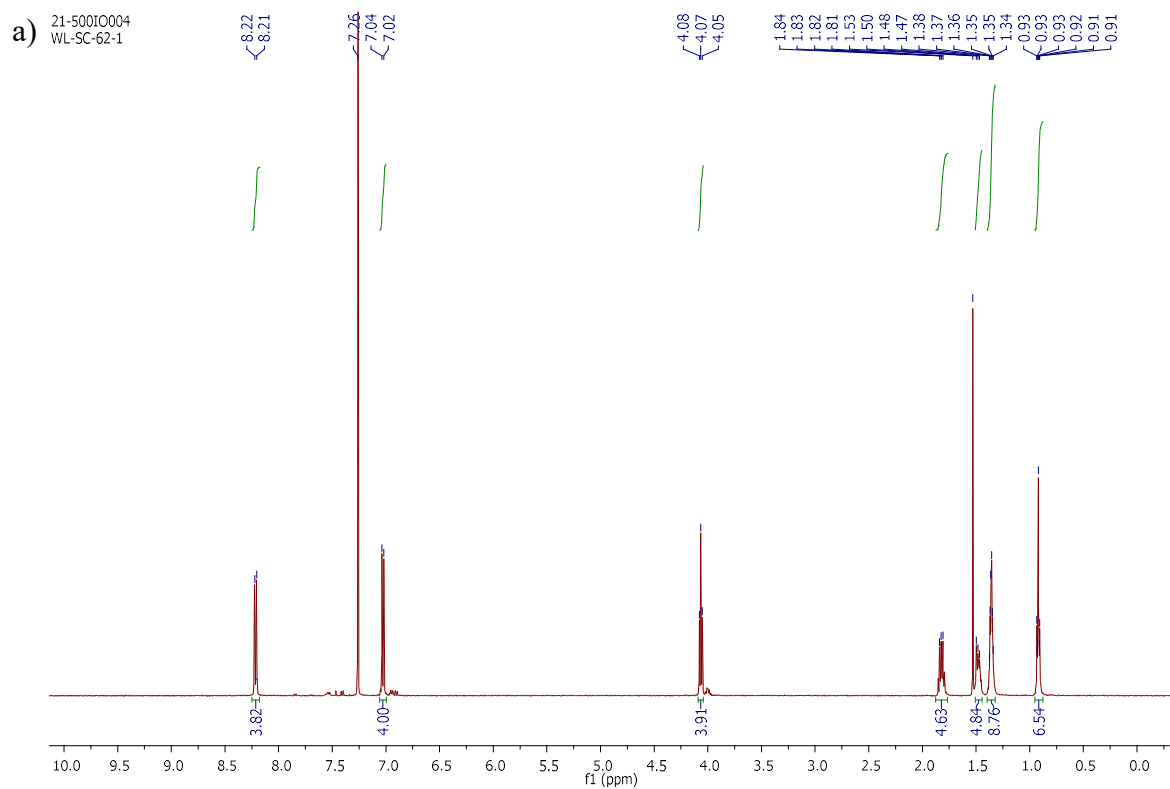


Figure S3 ^1H (a) and ^{13}C NMR (b) spectra of synthesized 3,6-bis(4-(hexyloxy)phenyl)furo[3,4-c]furan-1,4-dione (**5**) (6*O*,6*O*-*DDF*).

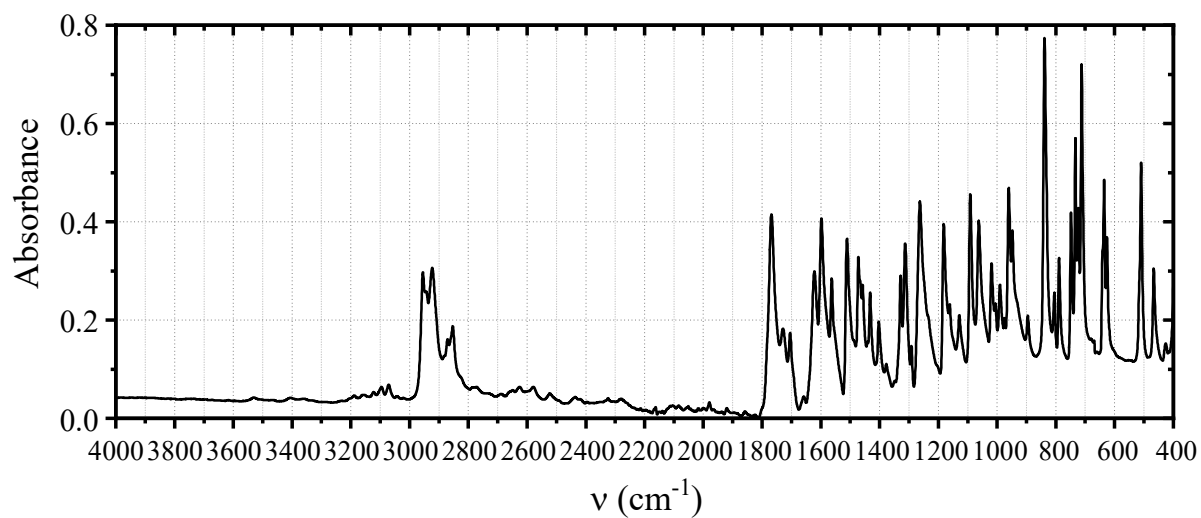


Figure S4 FTIR spectrum synthesized 3,6-bis(4-(hexyloxy)phenyl)furo[3,4-c]furan-1,4-dione (6O,6O-DFE) dye (5) powder measured with ATR accessory.

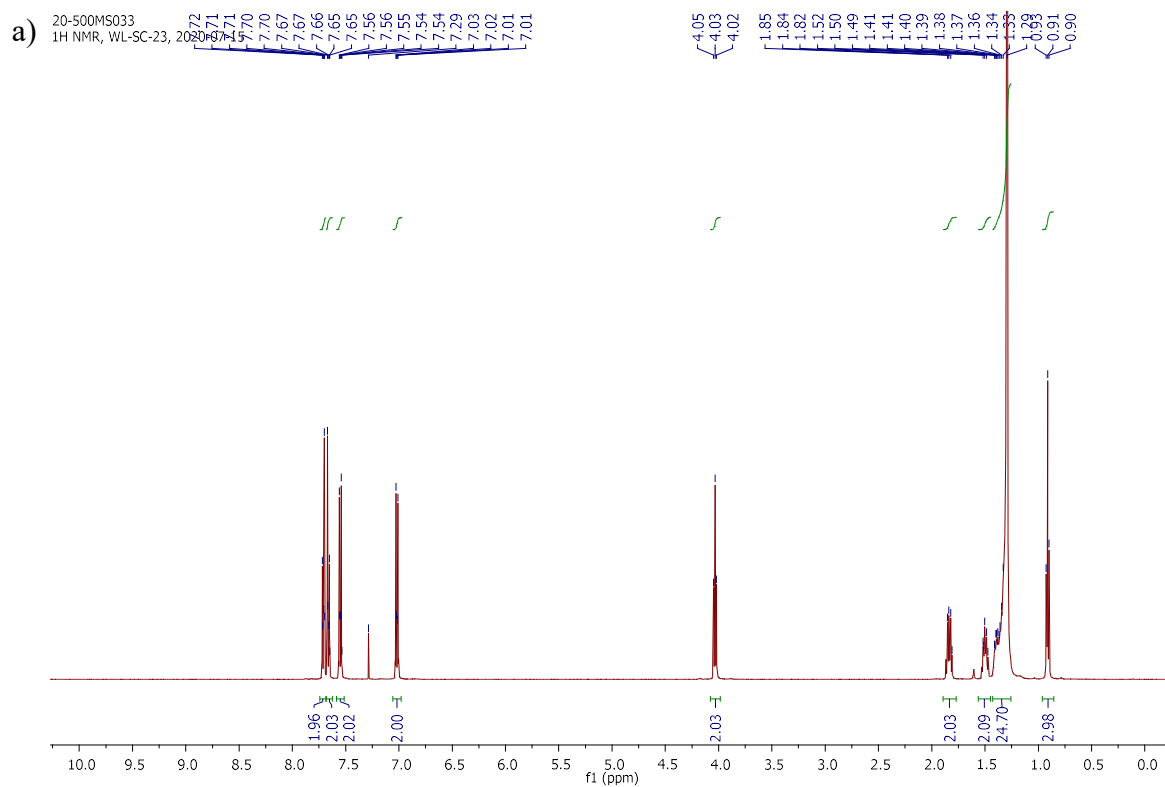


Figure S5 ¹H (a) and ¹³C NMR (b) spectra of synthesized 4'-(hexadecyloxy)-[1,1'-biphenyl]-4-carbonitrile (16OCB) (continued on the next page).

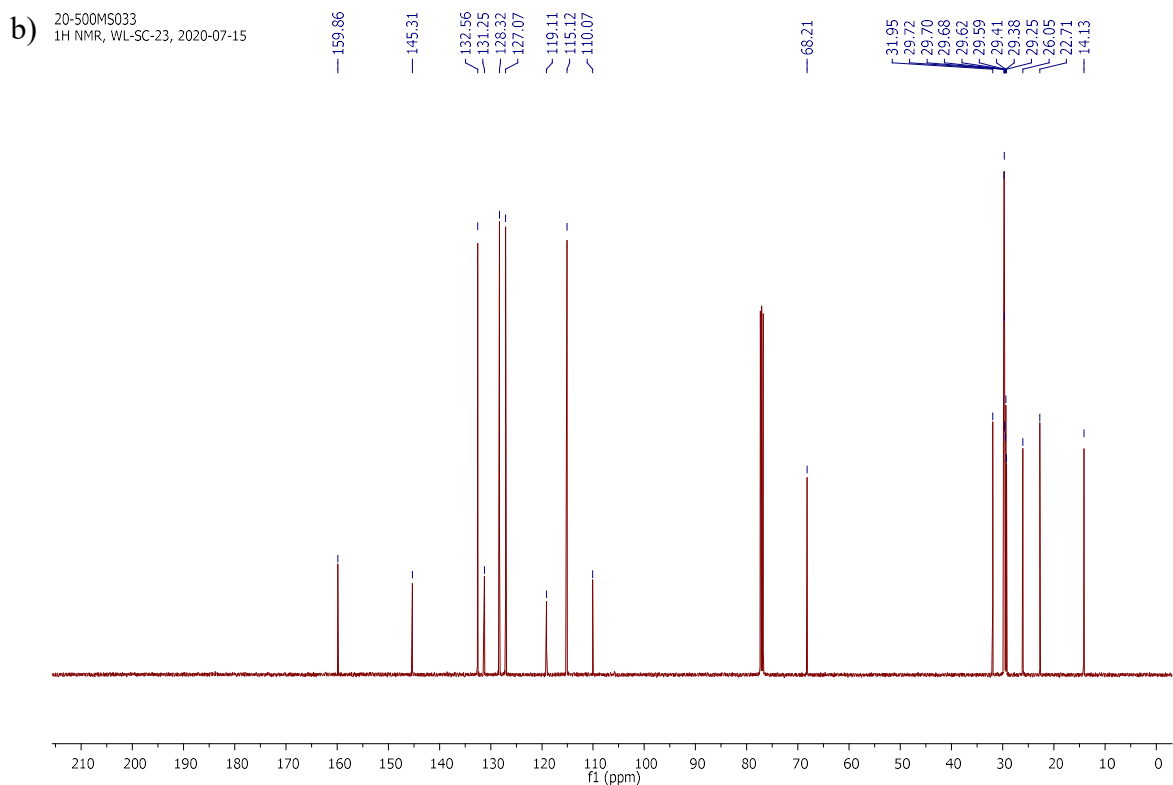


Figure S5 (continued) ^1H (a) and ^{13}C NMR (b) spectra of synthesized 4'-(hexadecyloxy)-[1,1'-biphenyl]-4-carbonitrile (*16OCB*).

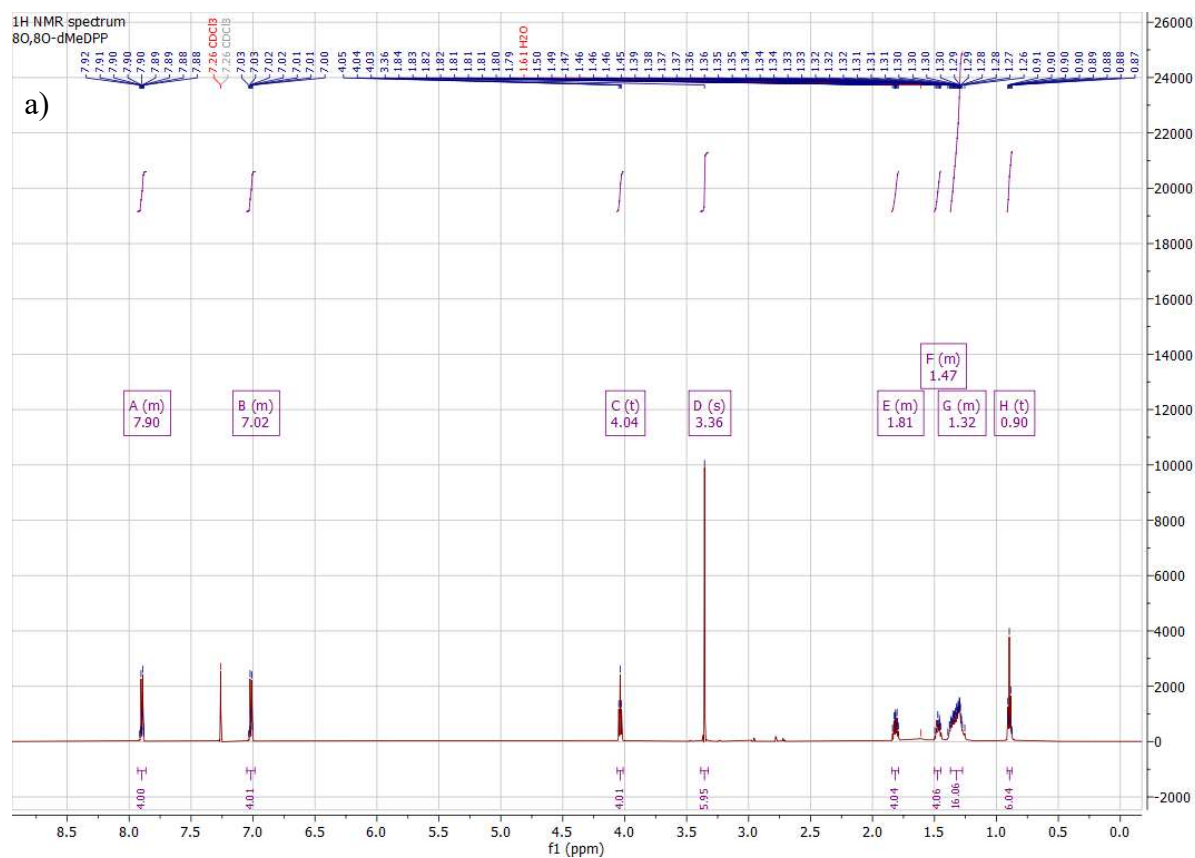


Figure S6 ^1H (a) and ^{13}C NMR (b) spectra of the synthesized 3,6-bis(4-octyloxyphenyl)-2,5-dimethyl-2,5-dihydropyrrolo[3,4-c]pyrrole-1,4-dione (*80,80-dMeDPP*) dye (continued on the next page).

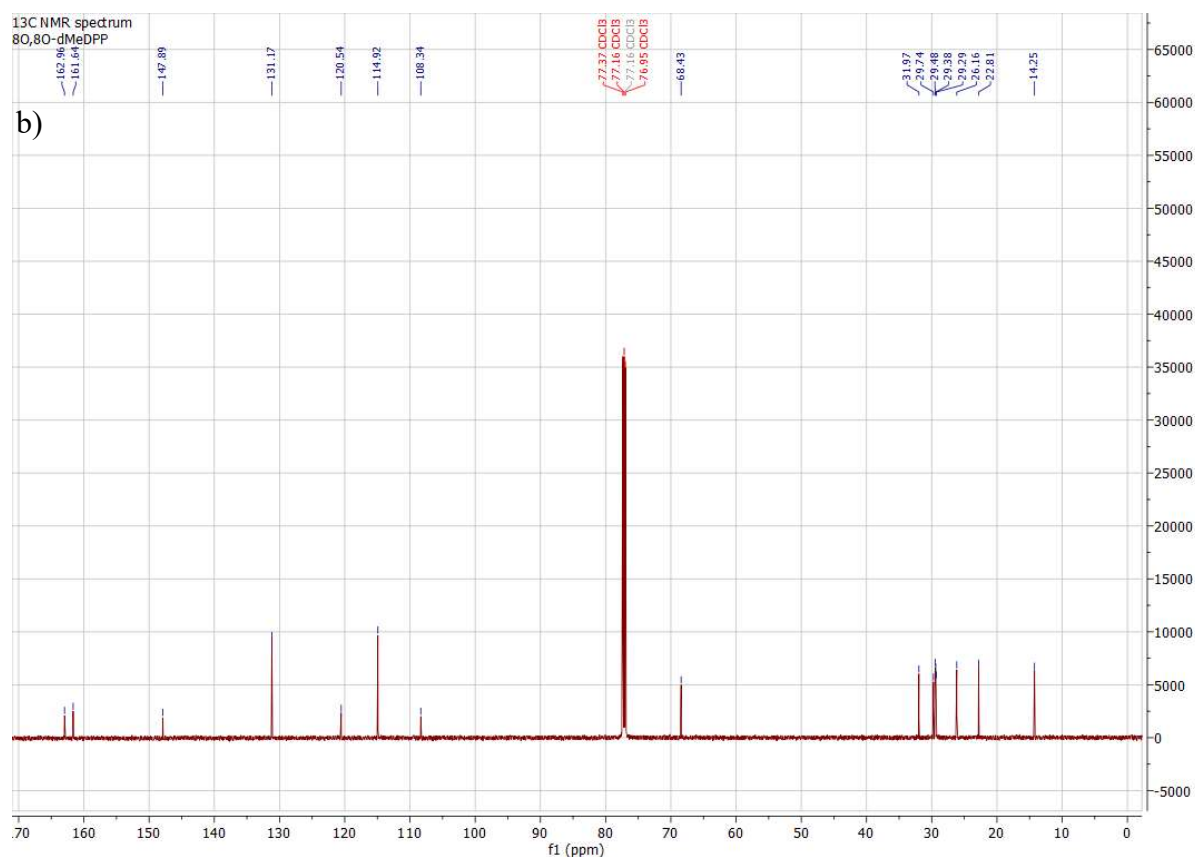


Figure S6 (continued). ^1H (a) and ^{13}C NMR (b) spectra of the synthesized 3,6-bis(4-octyloxyphenyl)-2,5-dimethyl-2,5-dihydropyrrolo[3,4-c]pyrrole-1,4-dione (*8O,8O-dMeDPP*) dye

S2. Crystal structure analysis

Table S1 Crystal data, data collection and structure refinement of the *6O,6O-DFP* dye single crystal.

Chemical formula	$\text{C}_{30}\text{H}_{34}\text{O}_6$
M	490.59
Crystal system, space group	Triclinic, $P\bar{1}$
a, b, c (Å)	5.3226(10), 7.1359(12), 16.897(3)
α, β, γ (°)	95.40(2), 90.29(2), 96.87(2)
V (Å ³)	634.3(2)
Z	1
T (K)	100(2)
Radiation type	$\text{CuK}\alpha$, $\lambda = 1.5418$ Å
μ (mm ⁻¹)	0.72
Crystal size (mm)	$0.07 \times 0.17 \times 0.22$
T_{\min}, T_{\max}	0.469, 1.00
No. of measured, independent, observed [$I > 2\sigma(I)$] reflections	22149, 2579, 2269
R_{int}	0.0453
R_1 [$F_0 > 4\sigma(F_0)$], wR_2, S	0.039 (observed refl.), 0.111 (all data), 1.07
No. of reflections	2579
No. of parameters	165
$\Delta\rho_{\text{max}}, \Delta\rho_{\text{min}}$ (e/Å ³)	0.30, -0.24

Table S2 Selected geometric parameters of the dye compound *6O,6O-DFP* determined in the single crystal.

Bond length (Å)		Bond angle (deg)		Torsion angle (deg)	
C1-C2	1.5256(18)	O1-C7-C12	124.33(10)	C6-O1-C7-C12	-0.45(16)
C2-C3	1.5229(16)	C11-C10-C13	121.46(11)	C11-C10-C13-C14	-177.12(12)
O1-C6	1.4458(13)	O2-C13-C10	117.59(10)	C13-O2-C15-O3	179.92(10)
O1-C7	1.3548(14)	O2-C15-O3	119.85(10)		
C7-C12	1.3962(17)				
C7-C8	1.4063(16)				
C8-C9	1.3767(17)				
C10-C13	1.4350(17)				
O2-C13	1.3902(14)				
C14-C14 ⁱ	1.419(2)				
C15-O3	1.2044(15)				
C15-O2	1.4194(14)				

ⁱ symmetry code: 1-x, 1-y, 1-z

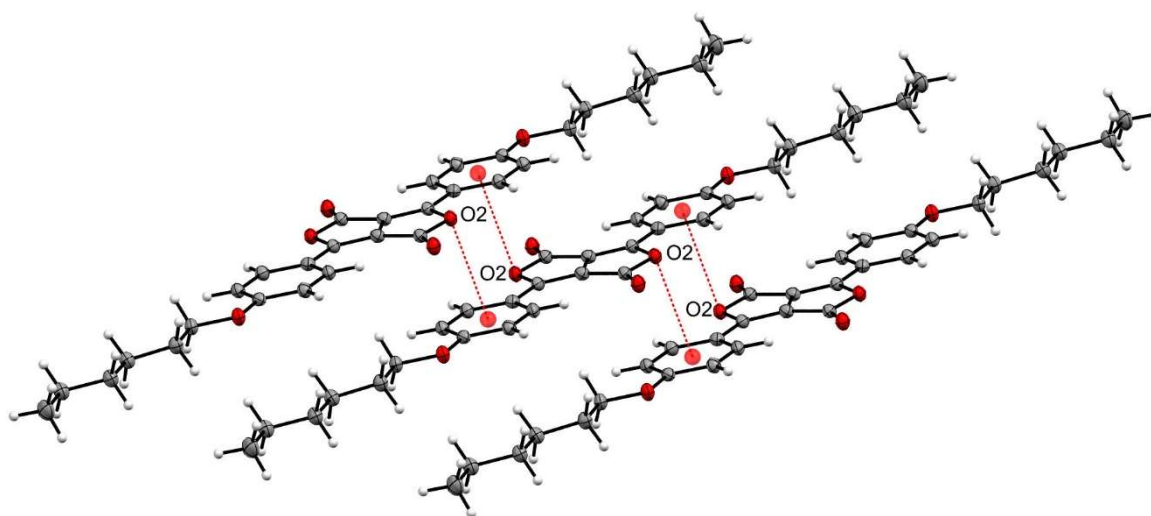


Figure S7 Selected *6O,6O-DFP* dye molecules stacked onto each other. Red dotted line indicates the distance between O2 and centroid of phenylene ring.

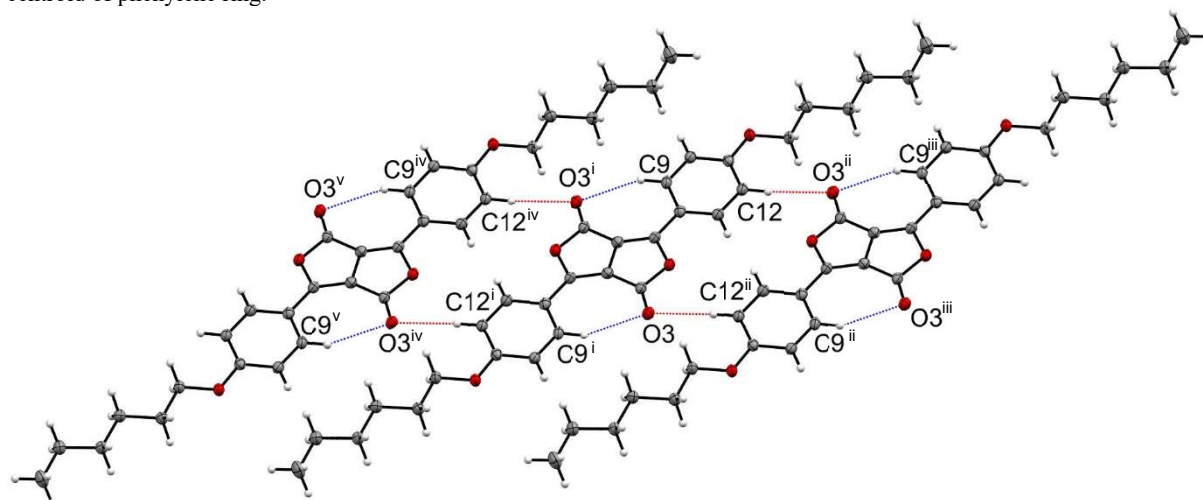


Figure S8 Possible intramolecular interactions (blue dotted lines) and intermolecular interactions between adjacent molecules of the *6O,6O-DFP* dye compounds (red dotted lines). Symmetry codes: (i) 1-x, 1-y, 1-z, (ii) -x, 2-y, 1-z, (iii) -1+x, 1+y, +z, (iv) 1+x, -1+y, +z, (v) 2-x, -y, 1-z

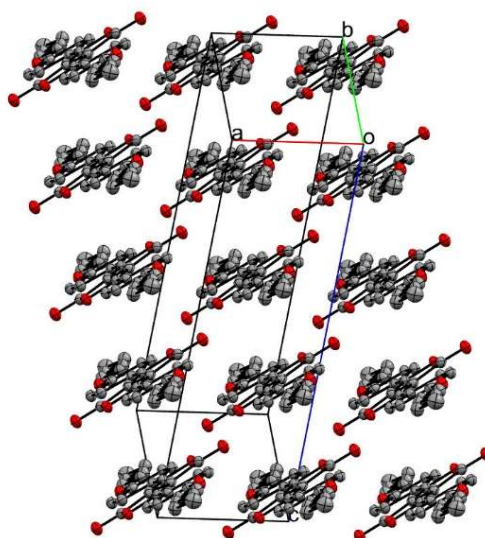


Figure S9 Crystal packing of the *6O,6O-DFP* dye molecules with cell axis.

S3. Thermal properties of thermotropic LCs and their mixtures

Table S3 Phase transition temperatures of the mixtures, dyes and LCs determined by Polarized Optical Microscopy or DSC (where marked). Routine uncertainty of the results was estimated to around 0.5°C for temperatures below 100°C and around 2°C close to 250°C.

Sample	Phase transition temperatures [°C]	Reference
0.1% <i>6O,6O-DFP</i> in <i>ZLI-1496</i>	<i>Cr</i> 49.6 <i>N</i> 81.5 <i>I</i>	this work
<i>ZLI-1496</i>	<i>Cr</i> 49.6 <i>N</i> 81.1 <i>I</i>	this work
	<i>Cr</i> 49.0 <i>N</i> 79.8 <i>I</i>	[5]
0.1% <i>6O,6O-DFP</i> in <i>16OCB</i>	<i>Cr</i> 81.5 <i>SmA</i> 93.9 <i>I</i>	this work
<i>16OCB</i>	<i>Cr</i> 81.8 <i>SmA</i> 93.7 <i>I</i>	this work
	<i>Cr</i> 81 <i>SmA</i> 91 <i>I</i>	[6]
<i>6O,6O-DFP</i>	<i>Cr</i> 242 ± 2 <i>I</i>	this work
	<i>Cr</i> 233.8 (peak) 240.5 (full transition) <i>I</i> *	this work
	<i>Cr</i> 106 <i>N</i> 114 <i>I</i>	this work
<i>8O,8O-dMeDPP</i>	<i>Cr</i> 104.6 (peak) <i>N</i> 113.5 (full transition) <i>I</i> *	this work
	<i>Cr</i> 106.2 <i>N</i> 114.0 <i>I</i>	[7]

* results from DSC curves for 2nd heating cycle performed at 10 °C/min (Differential scanning calorimeter DSC1 (Mettler-Toledo))

⁵ S. Pestov, V.Vill, Liquid Crystals. In: Warlimont H, Martienssen W. Springer Handbook of Materials Data, 2nd Edition, Springer; 2008, 959–991.

⁶ G. J. Brownsey, A. J. Leadbetter, *Phys. Rev. Lett.* 1980, **44**(24), 1608-1612.

⁷ K. Praefcke, M. Jachmann, D. Blunk and M. Horn, *Liq. Cryst.*, 1998, **24**(1), 153.

S4. Spectrofluorometric measurements

S4.1. Supplementary emission and excitation spectra

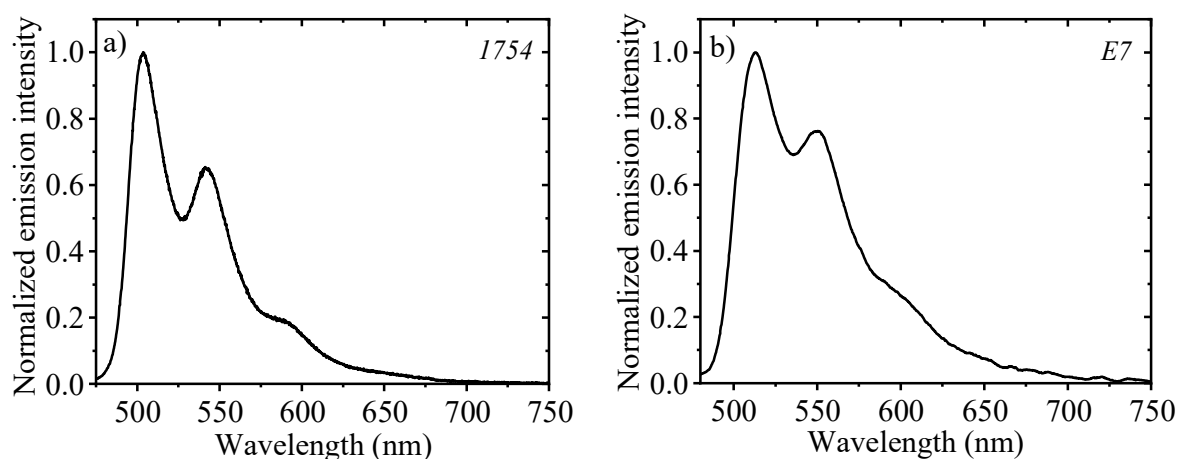


Figure S10 Emission spectra of diluted sample of the mixture of the *6O,6O-DFD* dye in the nematic LC hosts: a) *1754* (standard spectrofluorometer setup) and b) *E7* (setup with integrating sphere) at room temperature.

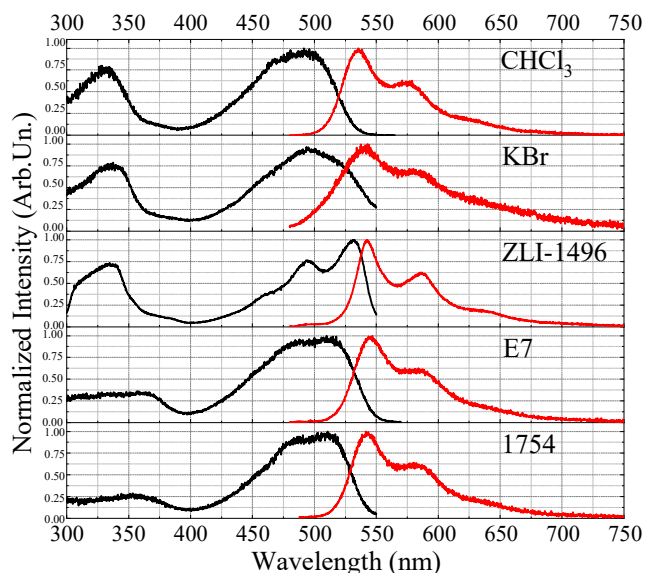


Figure S11 Excitation (black) and emission (red) spectra of diluted samples of the *8O,8O-dMeDPP* dye in various matrices, a) CHCl_3 (liquid) ($\lambda_{exc} = 470$ nm, $\lambda_{em} = 575$ nm), b) KBr (solid), $c = 0.001$ wt%, ($\lambda_{exc} = 460$ nm, $\lambda_{em} = 585$ nm), c) *ZLI-1496* (crystalline at RT), $c = 0.01$ wt%, ($\lambda_{exc} = 460$ nm, $\lambda_{em} = 585$ nm), d) *E7* (nematic at RT) $c = 0.001$ wt%. ($\lambda_{exc} = 470$ nm, $\lambda_{em} = 585$ nm), e) *1754* (nematic at RT), $c = 0.001$ wt% ($\lambda_{exc} = 460$ nm, $\lambda_{em} = 585$ nm).

S4.2. Spectroscopic analysis of presence of multiple forms of the 6O,6O-*DDF* dye in *ZLI-1496* matrix at RT

The excitation and emission spectra of the 0.01 % 6O,6O-*DDF* dye-doped *ZLI-1496* sample were registered (Fig. S12) for analysis of presence of multiple forms of the dye.

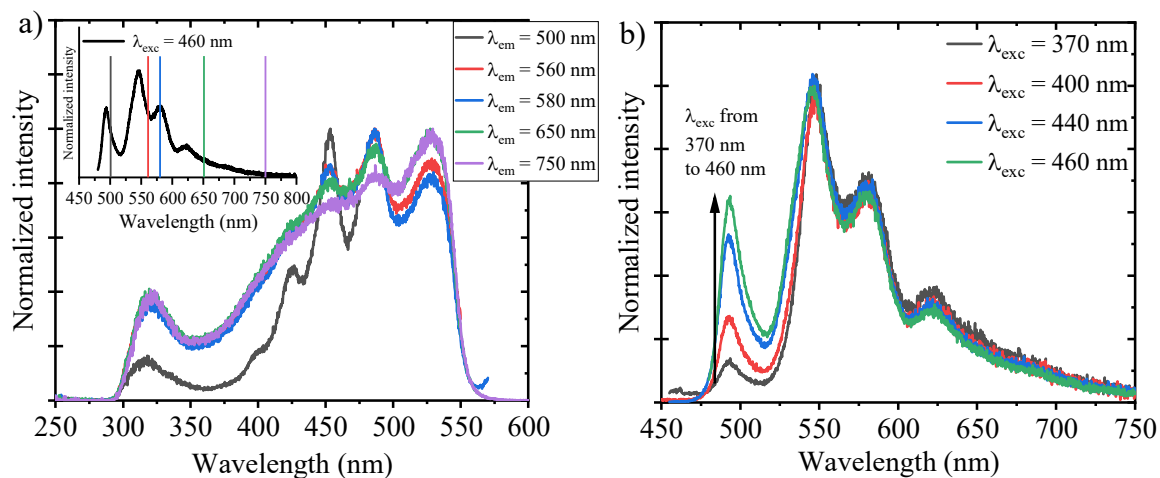


Figure S12 Dependence on a) excitation and b) emission spectra of the 0.01 % 6O,6O-*DDF* dye-doped *ZLI-1496* sample on a) emission, and b) excitation wavelength. Inset in Fig. (a) shows emission spectrum, registered for $\lambda_{exc} = 460$ nm with marked emission lines used for excitation spectra

The excitation and emission spectra of the 0.01 % 6O,6O-*DDF* dye-doped *ZLI-1496* sample differs in the shape, depending on the emission and excitation wavelength, respectively. It may indicate that more than one form of the dye is present in the sample. Taking into account, the results of the spectroscopic properties with the dilution of the dye, we assume that the dye may be in aggregated and separated state and these two forms may co-exist.

Excitation spectrum for $\lambda_{em} = 750$ nm (Fig. S12a) have stronger excitation band at 528 nm and much less distinct peaks at around 450 and 480 nm. The position of the excitation band corresponds to the position of the absorption band of the dye in the solid form of 0.1 wt% *ZLI-1496* sample (see Fig. S15f) and dispersed in KBr matrix (see Fig. 4b in the main text). Comparing the emission spectra in CHCl_3 solution and in KBr matrix (see Figs. 4a and 4b in the main text), the emission of the dye in the solid state is much more intense in the emission range from 700 to 800 nm. Thus, we suppose that the studied excitation spectrum for $\lambda_{em} = 750$ nm of 6O,6O-*DDF* dye-doped *ZLI-1496* sample may be much more intense for the solid (aggregated) form of a dye. From the other hand, excitation spectrum for $\lambda_{em} = 500$ nm is more similar to the excitation and absorption spectra of the CHCl_3 solution –their position of the maxima are similar and the bands are more sharp.

Emission spectra (Fig. S12b) differs in relative intensity of the band near 495 nm. The relative band intensity is very small for excitation wavelength for 370 nm, but it increases when changing the wavelength up to 460 nm. We refer the changes to different relative absorption of the separated and aggregated form of the dye. Comparing the excitation or absorption spectra of the dye in CHCl_3 solution and in KBr matrix (see Figs. 4a and 4b in the main text), the absorption of the solution is definitely much lower than that of the solid state sample in a range 350 – 380 nm. Then, the relative absorption between the solution and solid state sample increase with the wavelength. This led us to finding, that the emission signal at 495 is related only or much more to the separated form of the dye, which is supported by the emission spectra (see Fig. 4 in the main text).

S5. Characterization of thermofluorochromic properties of dye-doped thermotropic LCs

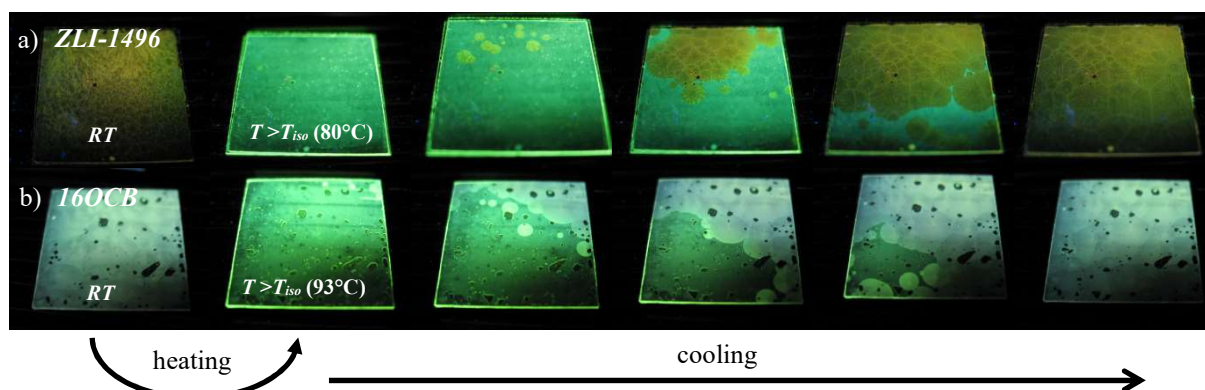


Figure S13 Comparison of thermofluorochromic behaviour under UV lamp of the mixtures of 0.1 wt% of the *6O,6O-DFE* dye with the *LC* hosts: a) *ZLI-1496* and b) *16OCB* enclosed between two cover microscopic glasses. The photographs from left to right were taken before and after heating above the isotropization temperature: 80 °C – in case of *ZLI-1496* and 93 °C – in case of *16OCB* (the first two photographs in the rows) and then subsequent upon inert cooling of the samples (consecutive four photographs) – presenting gradual crystallization over the whole area of the sample upon inert cooling. Note, that the blue colour emission in case of *16OCB* matrix is typical and related to emission of the *LC* host under excitation in the UV range.

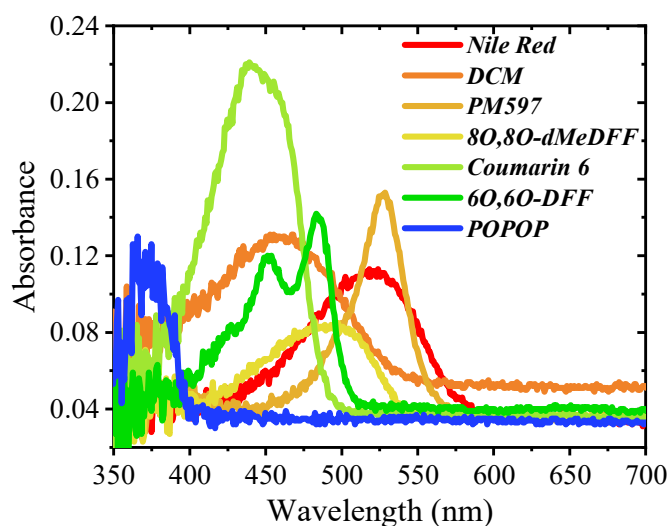


Figure S14 Absorption spectra of the samples of the dye-doped *ZLI-1496* 0.1 wt% mixtures in the isotropic state, related to the photographs presented in Fig. 7a in the main text.

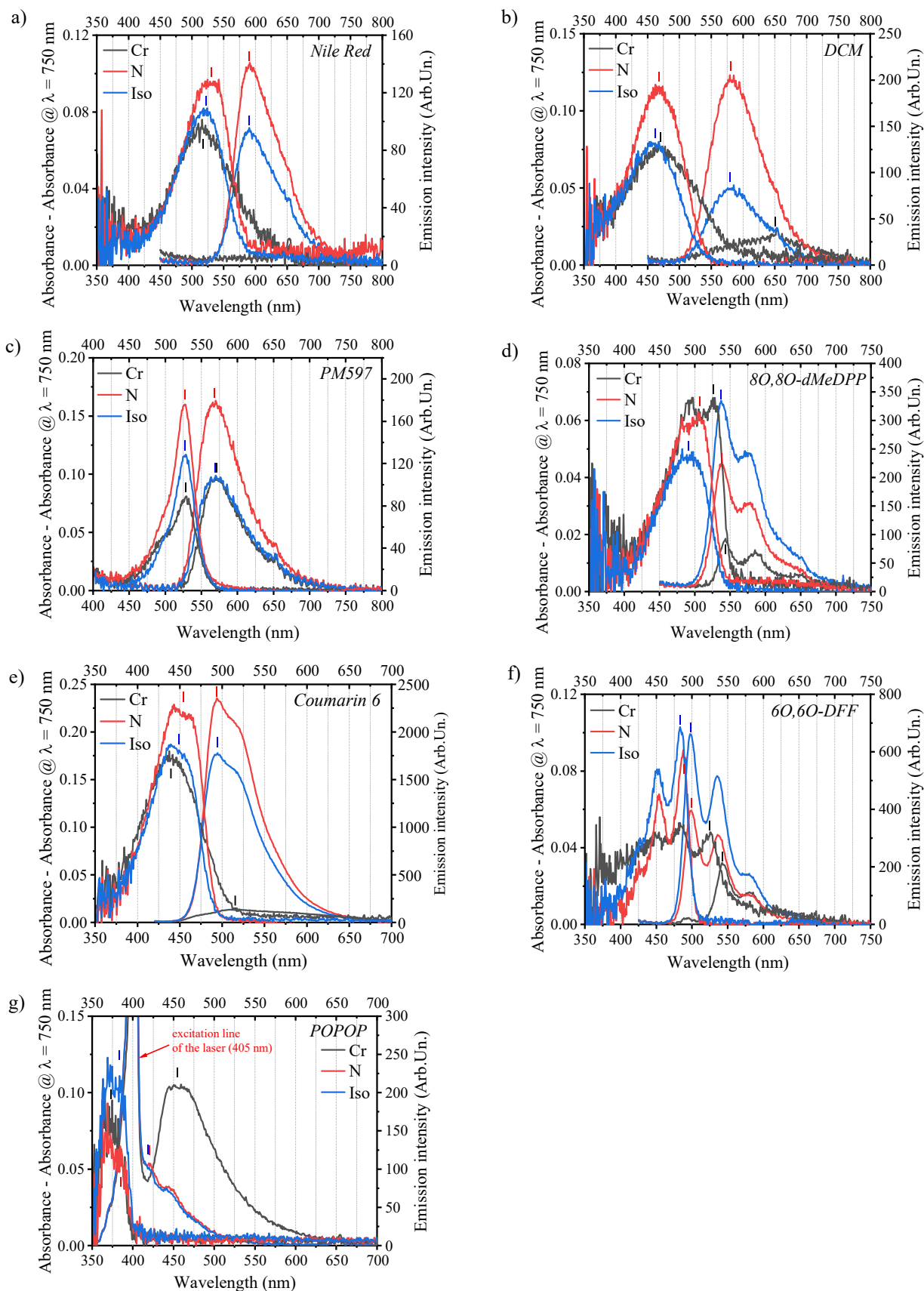


Figure S15 Series of absorption and emission spectra in different phases – crystalline (Cr), nematic (N) and isotropic (Iso) of 0.1 wt% dye-doped *ZLI-1496* LC cell, made of two clear glass slides. Positions of the maxima of the closest absorption and emission bands used for Stokes shift ($\Delta\nu_{Stokes}$) determination are marked with respective color above or below the proper maxima. The measurement were performed at 25 ± 5 °C (Cr), 65 ± 10 °C (N) and 85 ± 10 °C (Iso). Spectrum of the excitation line of the laser (405 nm) interferences with in the emission spectra of POPOP in Fig. (g) thus the range of 360–430 nm should not be taken into account in the analysis.

S.5.1. Analysis of the influence of Stokes shift and the absorption band position on the shift in emission band

On the basis of the spectra, the Stokes shifts ($\Delta\nu_{Stokes}$) between absorption and emission bands were determined in different phases and are summarized in Table S4. The results were also analysed in terms of shift of the absorption and emission band upon crystallization. Shift in the maxima of the absorption ($\Delta\nu_{abs,N-Cr}$) and emission ($|\Delta\nu_{em,max,N-Cr}|$) band, as well as shift in the edge of the absorption band ($|\Delta\nu_{abs,edge,N-Cr}|$) of the samples are listed in Table S5.

Absorption band edge was chosen as more relevant parameter than absorption maximum for the analysis of its influence on shift in the emission spectrum, because of different width of the absorption bands of the studied dyes. The results are depicted in Fig. 7c.

As the signal in case of *Nile Red* (dye with the highest contrast in emission intensity) was too small to read the position of the emission maximum in crystalline phase and in case of POPOP – the excitation line was partly superimposed with the emission spectra, the data was omitted in the graph.

Table S4 Summary of the position of maxima of closest absorption and the emission bands spectra for calculation of Stokes shift ($\Delta\nu_{Stokes}$) in 0.1 wt% dye-doped ZLI-1496 liquid crystal samples, according to the spectra presented in Fig. S15. The measurement were performed at 25 ± 5 °C (*Cr*), 65 ± 10 °C (*N*) and 85 ± 10 °C (*Iso*).

Dye	Phase	$\lambda_{abs,max}$ [nm]	$\lambda_{em,max}$ [nm]	$\Delta\nu_{Stokes}$ [cm ⁻¹]
<i>Nile Red</i>	<i>Cr</i>	516	n/d	n/d
	<i>N</i>	530	590	1919
	<i>Iso</i>	522	590	2208
<i>DCM</i>	<i>Cr</i>	470	651	5916
	<i>N</i>	468	581	4156
	<i>Iso</i>	462	579	4374
<i>PM597</i>	<i>Cr</i>	528	571	1426
	<i>N</i>	527	568	1370
	<i>Iso</i>	527	569	1401
<i>8O,8O-dMeDPP</i>	<i>Cr</i>	527	543	559
	<i>N</i>	507	538	1137
	<i>Iso</i>	494	537	1621
<i>Coumarin 6</i>	<i>Cr</i>	439	515	3362
	<i>N</i>	453	494	1832
	<i>Iso</i>	448	494	2079
<i>6O,6O-DFF</i>	<i>Cr</i>	525	542	597
	<i>N</i>	489	499	410
	<i>Iso</i>	484	499	621
<i>POPOP</i>	<i>Cr</i>	$372 \pm 5^*$	$454 \pm 5^*$	4855
	<i>N</i>	$384 \pm 5^*$	$419 \pm 40^*$	2175
	<i>Iso</i>	$383 \pm 5^*$	$420 \pm 40^*$	2300

* - uncertainty of reading of the maximum of the band position

Table S5 Summary of the shifts in the position of the maxima of the absorption bands ($\Delta\nu_{abs,N-Cr}$), position of the edge of the absorption bands ($|\Delta\nu_{abs,edge,N-Cr}|$) and maxima of the emission bands ($|\Delta\nu_{em,max,N-Cr}|$) upon crystallization of 0.1 wt% dye-doped ZLI-1496 liquid crystal samples, according to the spectra presented in Fig. S15.

Dye	$\Delta\nu_{abs,N-Cr}$ [cm ⁻¹]*	$ \Delta\nu_{abs,edge,N-Cr} $ [cm ⁻¹]	$ \Delta\nu_{em,max,N-Cr} $ [cm ⁻¹]
<i>Nile Red</i>	512	1094	n/d
<i>DCM</i>	-91	1371	1851
<i>PM597</i>	-36	291	92
<i>8O,8O-dMeDPP</i>	-749	403	171
<i>Coumarin 6</i>	704	638	825
<i>6O,6O-DFF</i>	-1402	1647	1590
<i>POPOP</i>	840	0	1840**

* minus sign in case of $\Delta\nu_{abs,N-Cr}$ refers to red-shift upon crystallization. Please note a red-shift in absorption edge as well as emission maximum upon crystallization

** the data for *POPOP* sample were omitted in further analysis, because of high uncertainty of the emission maxima position

S6. Studies of solubility of 6O,6O-DFE and 8O,8O-dMeDPP dyes in nematic LCs

Table S6 Results of polarized optical microscope observations of occurrence of 6O,6O-DFE dye microcrystals in the prepared mixtures with nematic LC hosts.

Matrix	Weight fraction of the dye (wt%)	Occurrence of the dye microcrystals			
		30 minutes after preparation	After 1 day	After 4 days	After 8 days
E7	0.5	Not clear	Yes	Yes	n/d
	0.25	Not clear	Yes	Yes	n/d
	0.1	No	Yes	Yes	n/d
	0.05	No	No	Yes	n/d
	0.02	No	No	No	n/d
	0.01	No	No	No	n/d
1754	0.5	Yes	Yes	Yes	Yes
	0.25	Yes	Yes	Yes	Yes
	0.1	No	Yes	Yes	Yes
	0.05	No	No	No	Yes
	0.02	No	No	No	No
	0.01	No	No	No	No

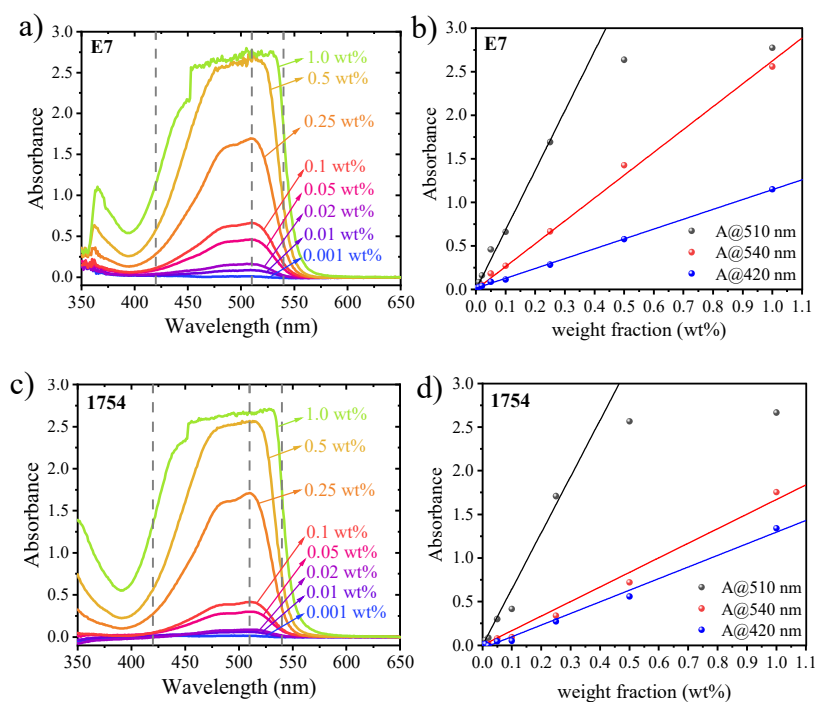


Figure S16. Results of the solubility studies of the 8O,8O-dMeDPP dye in LC nematic hosts: a, b) E7 and c, d) 1754 by UV-Vis absorption measurements. Reference samples were pure liquid crystals. The spectra were subtracted by the level of absorbance at 650 nm. Solid lines in b, d) present linear fits for proper series (only in case of A@540 nm – the linear fit refers only to the points in a range 0 – 0.25 wt%). Due to nonlinearity of absorbance with weight fraction at absorption maximum (at 510 nm) caused by technical limitation of the spectrophotometer the results at this wavelength were not taken into account in the analysis.

Table S7 Results of polarized optical microscope observations of occurrence of *8O,8O-dMeDPP* dye microcrystals in the prepared mixtures with nematic LC hosts.

Matrix	Weight fraction of the dye (wt%)	Occurrence of the dye microcrystals	
		On the day of preparation	After 3 days
E7	1.0	Yes	Yes
	0.5	Yes	Yes
	0.25	Not clear	Not clear
	0.1	No	Not clear
	0.05	No	No
	0.02	No	No
	0.001	No	No
1754	1.0	Yes	n/d
	0.5	Yes	n/d
	0.25	Not clear	n/d
	0.1	Not clear	n/d
	0.05	No	n/d
	0.02	No	n/d
	0.001	No	n/d

S7. Studies of light amplification of the cholesteric LC cells doped with *8O,8O-dMeDPP* dye

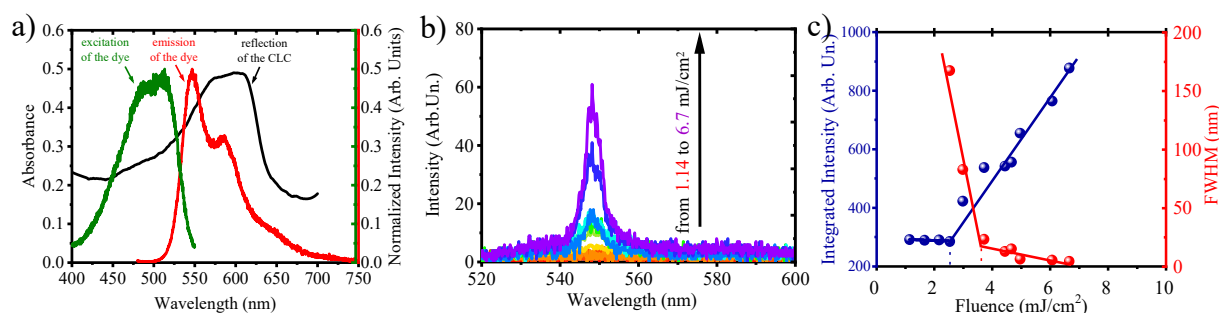


Figure S17. a) Absorption (black) spectrum of the 9.4 μm -thick cell filled with E7 + 39 wt% CB15 CLC mixture doped with 0.08 wt% of the *8O,8O-dMeDPP* dye. Red and green lines represent emission ($\lambda_{\text{exc}} = 460$ nm) and excitation ($\lambda_{\text{em}} = 585$ nm) spectra of the dye in E7 matrix at low excitation intensity, b) ASE spectra ($\lambda_{\text{exc}} = 480$ nm) of the dye-doped CLC cell with respect to pumping fluence and c) Light in - Light out and Full Width at Half Maximum characteristics of the *8O,8O-dMeDPP* dye-doped CLC cell.

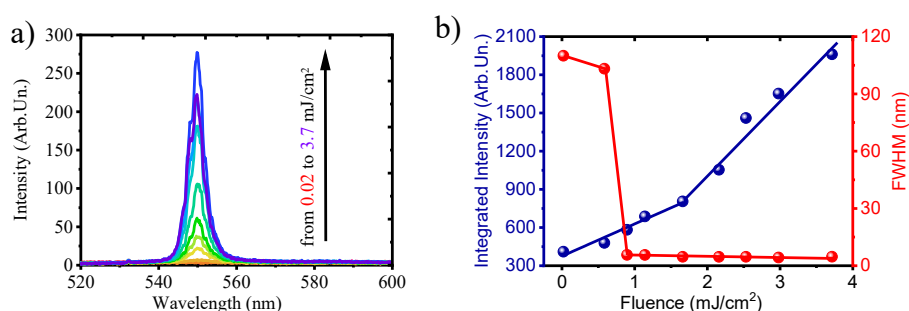


Figure S18. a) ASE spectra ($\lambda_{\text{exc}} = 480$ nm) with respect to pumping fluence of 9.6 μm -thick cell filled with E7 + 39 wt% CB15 CLC mixture doped with 0.23 wt% of the *8O,8O-dMeDPP* dye. b) Light in - Light out and Full Width at Half Maximum characteristics of the *8O,8O-dMeDPP* dye-doped CLC cell.